Local Endwall Heat/Mass-Transfer Distributions in Pin Fin Channels

S. C. Lau,* Y. S. Kim,† and J. C. Han‡
Texas A&M University, College Station, Texas

Naphthalene sublimination experiments were conducted to study the effects of the pin configuration, the pin length-to-diameter ratio, and the entrance length on local endwall heat/mass transfer in a channel with short pin fins (pin length-to-diameter ratios of 0.5 and 1.0). The detailed distributions of the local endwall heat/mass-transfer coefficient were obtained for staggered and aligned arrays of pin fins, for the spanwise pin spacing-to-diameter ratio of 2.5, and for streamwise pin spacing-to-diameter ratios of 1.25 and 2.5. The Reynolds numbers were kept at about 3.3×10^4. Overall- and row-averaged Nusselt numbers compared very well with those from previous heat-transfer studies.

Nomenclature

D = diameter of the pins
$\tilde{D}$ = diffusion coefficient of naphthalene
h_m = local mass-transfer coefficient, Eq. (1)
L = length of pins
L_e = entrance length
$\dot{m}''$ = local mass transfer per unit surface area per unit time
Nu = Nusselt number
Re_D = flow Reynolds number, Eq. (3)
S = distance between adjacent pins on a pin row in the spanwise direction
Sc = Schmidt number, Eq. (2)
Sh = Sherwood number, Eq. (2)
t = duration of a test run
$u_{\max}$ = average flow velocity evaluated at the minimum flow cross section, which is normal to the main flow direction
x = streamwise coordinate
X = distance between pins on adjacent rows in the streamwise direction
z = spanwise coordinate
Δy = change of the elevation at a measurement point
ν = kinetic viscosity of pure air
ρ_b = bulk naphthalene vapor density
ρ_s = density of solid naphthalene
ρ_w = naphthalene vapor density at a measurement point

Introduction

PIN fins have been used in the internal cooling channels at the trailing edge of gas turbine blades to increase the heat transfer to the cooling air (Fig. 1). The pins in these cooling channels are relatively short ($0.5 \le L/D \le 4$) due to the shapes of the blades and the various constraints commonly encountered during the blade manufacturing processes. Unlike the cross-flow heat exchangers ($L/D > 8$, for which the endwall heat transfer is negligible) and the plate-fin-and-tube compact heat exchangers ($L/D < 0.25$, in which the tube heat transfer is relatively small), the heat transfer from both the pins and the endwalls in the trailing-edge cooling channels of gas turbine blades contributes to the overall heat transfer to the cooling air. Although extensive heat-transfer studies have been conducted on channels with very long and very short pins,[1,2] the available experimental data cannot be interpolated to obtain the heat transfer in channels with pin fins of intermediate length-to-diameter ratios, which is of interest here.

VanFossen[3] studied the effect of the length-to-diameter ratio on the heat transfer from the pin and endwall surfaces in a channel with a four-row staggered array of short pin fins ($L/D = 0.5$ and 2). He found that the overall heat-transfer coefficients were lower than the data available in the literature for longer pins ($L/D > 8$), but were about two times higher than those for a plain channel with no pins. Brigham and VanFossen[4] conducted similar experiments with staggered arrays (four and eight rows) of slightly longer pin fins ($L/D = 4$), and found that the overall heat-transfer coefficients were higher than those for shorter pin fins ($L/D = 0.5$ and 2). Based on their results as well as those available in the literature, they concluded that, for short pin fins ($L/D < 2$), the heat transfer was a function of the Reynolds number only, whereas the heat transfer for longer pin fins ($L/D > 2$) was a function of both the length-to-diameter ratio and the Reynolds number.

Metzger et al.[5] investigated the heat transfer for channels with staggered arrays ($S/D = 2.5$, $X/D = 2.5$ and 1.25) of short pin fins ($L/D = 1$). The test section was made of 10 pin-row segments. Each individually heated segment consisted of two copper bars joined together with one row of copper pins, and was separated from the adjacent segments with plastic spacers. They found that, for all of the cases studied, the spanwise-averaged heat transfer increased in the streamwise direction until it reached its maximum value at about the third to the fifth row, then decreased gradually through the rest of the array. In Ref. 6, Metzger and Haley studied the effect on the pin fin channel heat transfer of replacing the copper (conducting) pins in the test section of Ref. 5 with wooden (nonconducting) pins. They found that the streamwise variation of the row-averaged heat transfer in the nonconducting pin case was similar to that in the conducting pin case. The overall heat transfer in the wooden pin case was lower than the previous case at high Reynolds numbers, and was higher at low Reynolds numbers. By measuring the local heat transfer from the pin surface and by hot-wire measurements, Metzger and Haley also demonstrated that the average pin Nusselt number and the turbulence intensity displayed

Received Aug. 22, 1986; revision received Dec. 12, 1986.
*Assistant Professor, Department of Mechanical Engineering.
†Research Assistant, Department of Mechanical Engineering.
‡Associate Professor, Department of Mechanical Engineering.

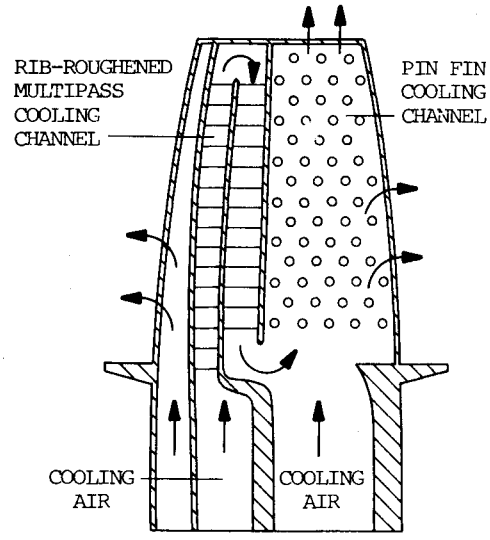

Fig. 1 Cutaway view of a typical modern internally cooled gas turbine blade.

similar increasing then decreasing trends as that of the streamwise distribution of the spanwise-averaged heat-transfer coefficient.

Simoneau and VanFossen[7] conducted experiments to measure the heat transfer from a heated pin fin ($L/D = 3$) that was placed at various locations in staggered and in-line arrays of identical unheated pins in a rectangular channel. The spanwise turbulence intensity profiles immediately upstream of the row containing the heated pin were also measured. They reported that both the heat transfer from the pin and the average turbulence intensity for the staggered arrays increased then decreased with increasing number of rows of pins upstream of the heated pin. The results were consistent with those reported in Refs. 5 and 6.

In Refs. 3–6, the average heat-transfer coefficients in short pin fin channels were determined. However, the distributions of the local heat-transfer coefficient on the pin and endwall surfaces were not studied.

Saboya and Sparrow[8,9] measured the local heat/mass-transfer coefficients on the endwalls of one- and two-row pin fin channels via the naphthalene sublimination technique. Although their results, which were for pin fins of a very small length-to-diameter ratio ($L/D = 0.193$) and for low Reynolds numbers, may not be applied to the turbine blade pin fin channels, the mass-transfer technique they used provided a means to study local surface heat transfer in complicated internal flow situations. In Ref. 10, naphthalene sublimination experiments were carried out to study the effect of the flow Reynolds number on the local Sherwood number in a pin fin channel. The experimental results were presented for a staggered array ($S/D = X/D = 2.5$) of pin fins. The length-to-diameter ratio was kept at 1.0 and the Reynolds number range was from 0.9 to 3.3×10^4.

The present investigation is devoted to study, via the naphthalene sublimination technique, the effects of the pin configuration, the pin length-to-diameter ratio, and the entrance length on the local endwall heat/mass transfer in a pin fin channel, which resembles the cooling passage at the trailing edge of a typical gas turbine blade. The flow Reynolds number is maintained at about 3.3×10^4 to facilitate the comparison of data. To establish the reliability of the results of the present study, the local endwall mass-transfer data are averaged by rows as well as over the entire test channel endwall. The average data are then compared with results by Metzger et al.[5,6]

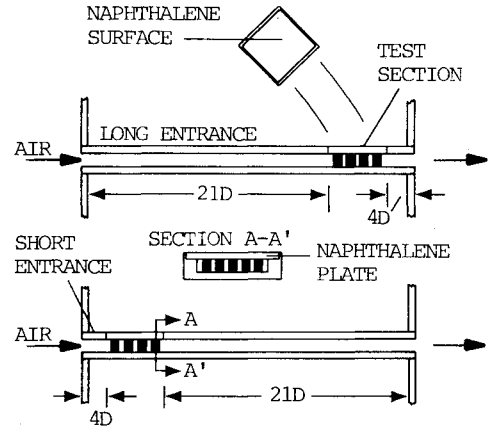

Fig. 2 Schematic of test channel (not to scale).

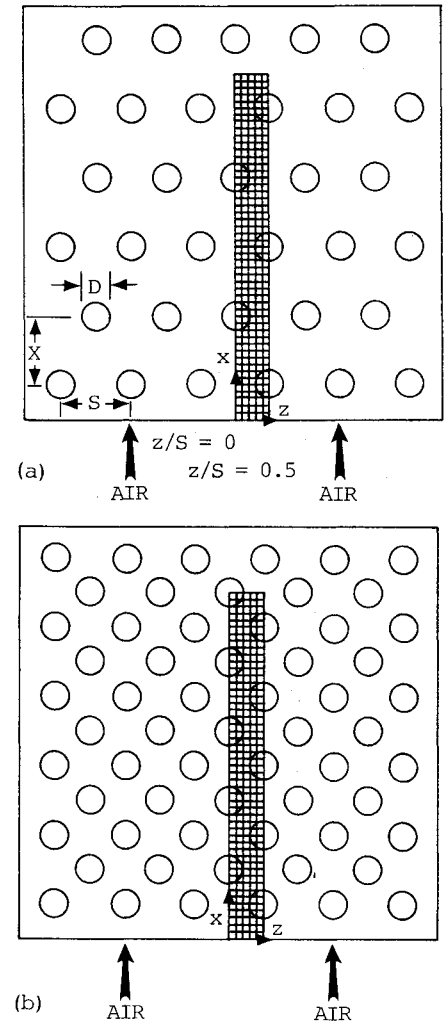

Fig. 3 Configurations of pin fin arrays: a) case 1; b) case 2.

Test Apparatus and Procedure

The experimental apparatus will now be described. The open flow loop was the same as previously employed in Ref. 10. The main component of the flow loop was a 0.26-m-long rectangular channel with a flow cross section of 9.53 cm × 6.35 mm. The bottom wall and the sidewalls of the channel were made of aluminum. As illustrated in Fig. 2, the test section was a 9.73-cm-long section of the channel with an array of 6.35-mm-long pin fins attached onto the bottom wall in either a staggered or an aligned fashion. While the top wall of the

channel was acrylic, the top wall of the test section was a naphthalene cassette.

The naphthalene cassette was a hollowed-out, 12.70-mm-thick, aluminum block with a 9.53-cm-square, flat, naphthalene surface, which was as smooth and as flat as the highly polished stainless-steel plate against which it was cast. The naphthalene surface was surrounded by two 6.35-mm-wide opposite edges and two other opposite edges 1.02 mm wide. When the cassette was installed on the test section, the two wide edges rested against the top of the sidewalls. The raised edges of the channel sidewalls and the top wall of the rest of the channel prevented any lateral movement of the naphthalene cassette once installed. Two large binder clips were used to hold the naphthalene cassette in place.

The pins were made from either 6.35 or 12.70-mm aluminum rods, depending on the height-to-diameter ratio being studied. The use of metallic pins instead of naphthalene pins should not affect the local endwall mass-transfer coefficient distribution directly, since the local endwall mass-transfer coefficient is dependent only on the pin configuration and the flow conditions. The pins were arranged in one of the four configurations as given in Table 1, in which the various cases studied in the present investigation are listed. Two typical configurations of the pin fin array (those of cases 1 and 2) are shown in Fig. 3. In case 1, there were five alternate spanwise rows of six pins and five pins in the array, while in case 2 there were nine pin rows (in both cases, the last pin row was not counted). The endwall heat/mass-transfer data were obtained at discrete points. These points formed a regular grid in a rectangular region near the middle of the pin fin array, as shown in Fig. 3. It should be pointed out that the aligned array of case 3 was achieved with the removal of alternate pin rows from the array of case 2 and that there were only three rows of pins (two rows of three pins and one row of two pins) in the array of case 4.

Air leakage between the top of the pins and the naphthalene surface during test runs was prevented by 0.64-mm-thick rubber gaskets installed on top of the pins.

The test section was 13.34 cm and 2.54 cm (equivalent to 21 and 4 times the pin diameter) from the two ends of the channel, as shown in Fig. 2. Two large acrylic flanges, which were of the same dimensions, were attached to the two ends of the flow channel, respectively. This was to provide an abrupt contraction entrance to the flow channel and enable the attachment of the flow channel onto the settling chamber. By attaching the respective flanges onto the settling chamber, the study of the entrance length effect on the local endwall heat/mass transfer in the test section was made possible.

In each experiment, the distribution of the local mass-transfer coefficient was obtained by measuring the elevations at discrete points on the naphthalene surface before and after air was circulated through the test section. The elevation measurements were made with a Starrett Model 812 electronic depth gage that had an accuracy of 0.0001 mm. The depth gage consisted of an electronic unit with digital readouts and a sensing head. The sensing head was mounted on a fixed dial gage stand overhanging the coordinate table on which the naphthalene cassette was affixed. In order to ensure that elevation measurements were made at the same points on the naphthalene surface before and after each experiment, the naphthalene cassette had to be mounted on the coordinate table at exactly the same position before and after each experiment. This was accomplished through the construction of an aluminum fixture with a slot that had the same dimensions as the naphthalene cassette. The fixture was bolted down onto the coordinate table. Therefore, it was possible to place the cassette at exactly the same position with respect to the coordinate table once the cassette was installed in the slot.

Before and after each experiment, the elevations at 300 points (or 600 points—6 points in the spanwise direction, 50 or 100 points in the streamwise direction) were measured in a region on the naphthalene surface, as shown in Fig. 3. In addition, elevation measurements were made on the two opposite, thin, aluminum frames. These measurements provided reference points to correct for the slight tilting of the naphthalene plate with respect to the coordinate table surface. A computer program was written to determine the elevation at each measurement point with respect to the elevations at the aforementioned reference points. Thus, the actual change of the elevation at each measurement point during the experiment could be calculated.

Prior to each test run, a naphthalene plate was prepared from fresh crystalline naphthalene. The naphthalene plate was then kept in a sealed plastic bag in the air-conditioned laboratory for a period of at least 12 h, so that it would attain the temperature of the laboratory, which was always maintained at 21.1°C ± 0.6°C. Other preparatory steps included warming up the blowers and presetting the valves to obtain the desired flow rate. Before the initial elevation measurements were made, the naphthalene plate was installed on the test section for 5–10 min. This procedure was necessary to ensure that the surface contour calculation did not include any deformation of the naphthalene surface caused by pressure exerted by the pins on the naphthalene surface.

During the test run, the pressure drop across the orifice plate, the static pressure upstream of the orifice plate, the temperature of the air flowing through the test section, and the atmospheric pressure were measured and recorded periodically. The duration of the test run was recorded with a stopwatch.

Supplementary experiments were also performed to determine the effect of natural convection during the elevation measurements and to establish that the procedures followed in the present investigation produced results comparable to previously published results.

Table 1 Pin configurations, entrance lengths, and Reynolds numbers for various cases studied

Case	X/D	S/D	L/D	Pin arrangement	L_e/D	$Re_{D_h} \times 10^4$
1	2.5	2.5	1.0	Staggered	21	3.3
2	1.25	2.5	1.0	Staggered	21	3.0
3	2.5	2.5	1.0	Aligned	21	3.3
4	2.5	2.5	0.5	Staggered	21	3.4
5	2.5	2.5	1.0	Staggered	4	3.3

Data Reduction

The local mass-transfer coefficient at each of the 300 (600 for some test runs) measurement points was determined from the measured change of the elevation at the point (Δy), the duration of the experiment (t), the density of solid naphthalene (ρ_s), and the difference between the naphthalene vapor density at the measurement point (ρ_w) and the bulk naphthalene vapor density (ρ_b).

$$h_m = \dot{m}''/(\rho_w - \rho_b) = \rho_s \Delta y/[(\rho_w - \rho_b)t] \qquad (1)$$

The bulk naphthalene vapor density (the cumulative mass of naphthalene in the airstream divided by the air volumetric flow rate) and the naphthalene vapor density at the measurement point were calculated as in Refs. 8 and 9. Because of the relatively short test section and the high airflow rates used in the present investigation, the bulk naphthalene vapor density was very small compared with the naphthalene vapor density at the wall. The values of ρ_b never exceeded 0.5% of ρ_w. Therefore, although the use of metallic pins instead of naphthalene pins lowered the cumulative mass of naphthalene in the airstream, the effect of using metallic pins on the calculation of the local endwall mass-transfer coefficient was negligible.

The local Sherwood number was defined as the product of the local mass-transfer coefficient and the pin diameter divided by the diffusion coefficient of naphthalene. The diffusion coefficient was calculated by dividing the kinematic viscosity of pure air by the Schmidt number of naphthalene.

$$Sh = h_m D/\tilde{D} = h_m D/(\nu/Sc) \quad (2)$$

The flow Reynolds number was based on the maximum air velocity, the pin diameter, and the kinematic viscosity of air.

$$Re_D = u_{\max} D/\nu \quad (3)$$

The velocity in the preceding equation was evaluated by dividing the volumetric flow rate by the area of the minimum flow cross section, which was normal to the main flow direction.

By using the maximum uncertainties for $(\rho_w - \rho_b)$, ρ_s, Δy, and t of 6, 2, 4, and 3%, respectively, and the uncertainty estimation method of Kline and McClintock,[11] it was found that the maximum uncertainty for the calculated local Sherwood numbers was less than 8%.

Results and Discussion

The experimental results will now be presented. In preliminary tests, the axial distributions of the local Sherwood number along the centerline of the test-section channel with no pin installed were determined for Reynolds numbers (based on the hydraulic diameter of the channel) of 1.0 and 3.0×10^4. Both the long and the short entrance cases ($L_e/D = 21$ and 4) were examined. The fully developed Sherwood numbers for all four cases agreed with the corresponding values given in Ref. 12 to within 3%. For the long duct entrance cases, the local Sherwood number decreased monotonically to the asymptotic fully developed value with increasing axial distance, while for the short entrance cases the local Sherwood number increased sharply near the entrance, reached a maximum very rapidly, and then decreased to the fully developed value.

The streamwise distributions of the local Sherwood number for the various cases studied are plotted for values of z/S varying from 0 to 0.5 in Figs. 4, 6, 8, 10, and 11. In each figure, there are six ordinate scales—one for each of the distribution curves. The relative positions of the zeros of these scales correspond to the order in which the distribution curves are displayed. Below each set of graphs, a sketch indicates the streamwise as well as the spanwise coordinates, x and z. Furthermore, the sketch shows the pin configuration corresponding to the experimental data being plotted and the locations of the pins. In addition, typical two-dimensional distributions of the local Sherwood number for selected cases studied are given in Figs. 5, 7, and 9. Based on these results, the effects of the pin configuration, the pin height-to-diameter ratio, and the entrance length on the local endwall heat/mass transfer will be discussed.

Pin Configuration Effect

Experimental results for cases 1–3 are presented in Figs. 4–9. The pin configurations for the three cases were given in Table 1. The pin fins were staggered in cases 1 and 2, while they were aligned in case 3. In the first case, the local Sherwood number was determined at 300 points—6 and 50 points in the spanwise and the streamwise directions, respectively. In the latter two cases, twice as many points as in case 1 were measured—100 points—along the main flow direction. In case 2, the Reynolds number was 3.0×10^4, which was slightly lower than the Reynolds numbers of about 3.3×10^4 in the other two cases.

Attention will first be given to Fig. 4. It can be seen that, near the leading edge of the test section, the local Sherwood number decreases with increasing streamwise distance as the concentration boundary layer grows. The Sherwood number then increases as the flow encounters the pins on the first and second rows. The axial distributions of the Sherwood number between the pins on the second and fifth rows are nearly periodic, that is, the corresponding segments of the distributions have similar shapes. In general, the mass transfer is high immediately upstream of a pin and in the wake region downstream of a pin. The results are consistent with Goldstein and Karni's[13] description of a horseshoe vortex system near the base of a cylinder in crossflow.

Figure 5 shows the two-dimensional Sherwood number distribution for case 1 in a typical region between $x/X = 2.5$ and 3.5. It can be seen that there is a rapid rise of the Sherwood number upstream of a pin. The Sherwood number is generally large upstream of a pin as well as in a relatively large wake region downstream of a pin.

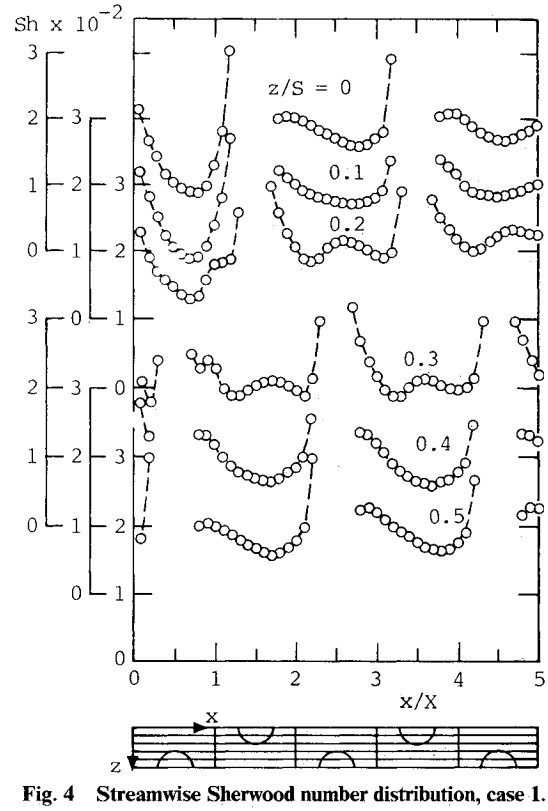

Fig. 4 Streamwise Sherwood number distribution, case 1.

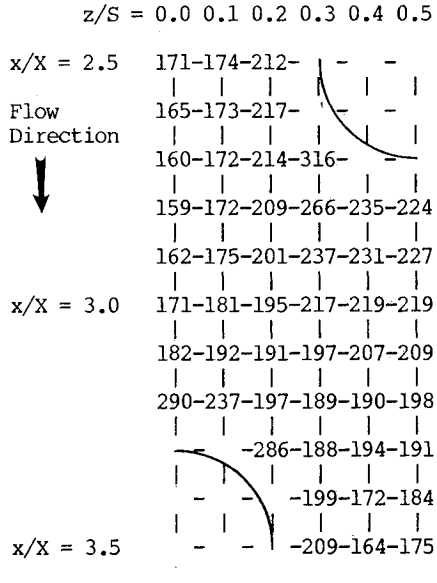

Fig. 5 Typical two-dimensional Sherwood number distribution, case 1.

The local Sherwood numbers in case 2, as shown in Fig. 6, are generally higher than those in case 1. Between the leading edge and the pins on the first and second rows, the streamwise Sherwood number distributions show the same trend of decreasing and then increasing in the main flow direction as in case 1. A close examination of the distributions for various z/S reveals that, with increasing x/X, the Sherwood number decreases along $z/S = 0.1$ faster than it does along $z/S = 0$. The initial drop of the Sherwood number near the leading edge along $z/S = 0.2$ is even larger than that along $z/S = 0.1$. Immediately upstream of the pin on the second row, the Sherwood number increases very rapidly along $z/S = 0$ and 0.1, less so along $z/S = 0.2$.

Between the leading edge and the pin on the first row, the Sherwood number along $z/S = 0.3$ decreases and then increases more gradually than it does along $z/S = 0.4$ and 0.5. Similar trends can be observed in Fig. 4, although they are not as consistent as those in Fig. 6. This is partly because the local Sherwood number was measured at only half as many points in the former case.

In Fig. 6, a peak in the Sherwood number distribution along $z/S = 0.2$ is evident at $x/X = 0.8$. Near the next two pins, the distribution curves behave rather erratically. Downstream of the fourth pin, the local Sherwood number distributions appear to have attained their periodic profiles. In Fig. 4, the existence of the first pin distorts the U shape of the distribution curve along $z/S = 0.2$ slightly at $x/X = 1.0$. The distribution curves in case 1 require only a short axial distance (x/X) for the development of the periodic profiles.

The two-dimensional Sherwood number distribution for case 2, as given in Fig. 7, shows the higher local mass transfer with a decrease in X/D from 2.5 to 1.25. As in Fig. 5, the local mass transfer in case 2 is high upstream of a pin and in the wake region downstream of a pin.

Next, the distributions of the local Sherwood number for an aligned array of pin fins (case 3) will be examined. In Fig. 8, the decrease in the Sherwood number near the leading edge is again caused by the growth of the concentration boundary layer. After the Sherwood numbers along $z/S = 0$ and 0.1 reach their minimum values at $x/X = 0.8$, they increase with increasing x/X, and then level off gradually. Downstream of $x/X = 2.0$, the Sherwood number appears to be independent of the streamwise coordinate. The difference between these distributions and the axial heat/mass-transfer distribution for flow in a plain rectangular channel may be caused by the increase in the flow velocity due to the flow blockage and the high turbulence level in the pin fin channel. Unlike the axial Sherwood number distributions along $z/S = 0$ and 0.1, the distribution along $z/S = 0.2$ has approximately periodic peaks, which are believed to be caused by the secondary flow induced by the nearby pins.

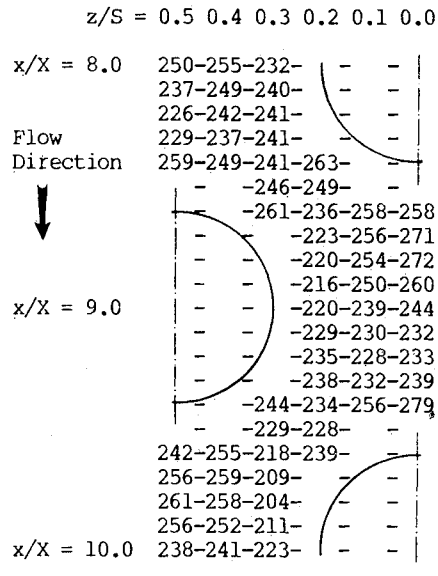

Fig. 7 Typical two-dimensional Sherwood number distribution, case 2.

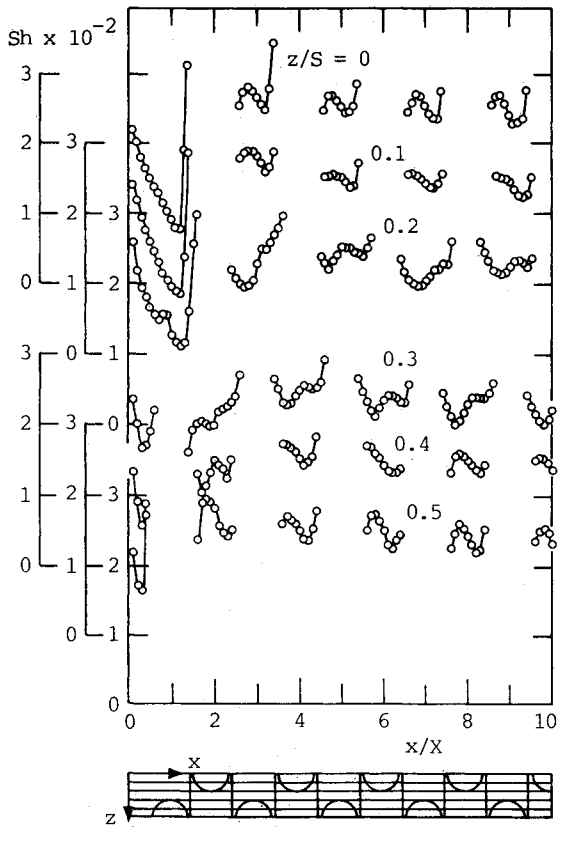

Fig. 6 Streamwise Sherwood number distribution, case 2.

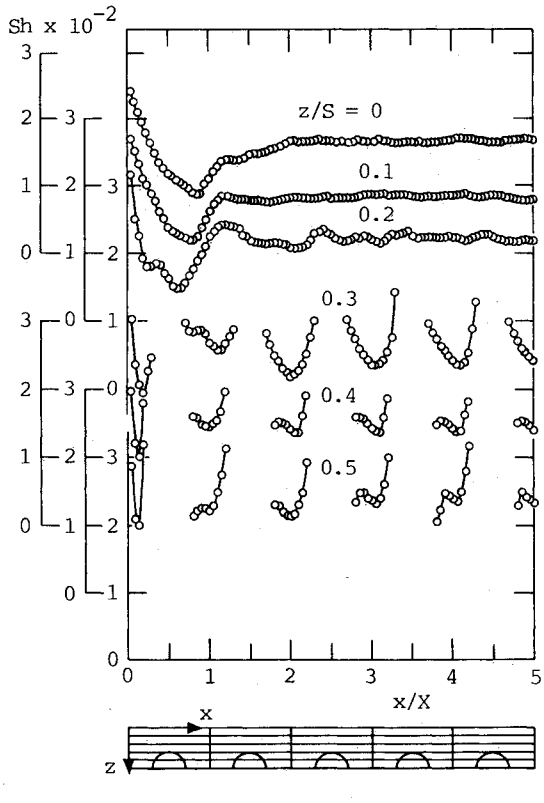

Fig. 8 Streamwise Sherwood number distribution, case 3.

Table 2 Spanwise-averaged Sherwood numbers and Nusselt numbers of Cases 1 and 2

	Case 1 $Re_D = 3.3 \times 10^4$		Case 2 $Re_D = 3.0 \times 10^4$	
Row	$\overline{Sh}$	$\overline{Nu}$	$\overline{Sh}$	$\overline{Nu}$
1	166.6	100.1	169.9	102.1
2	194.6	117.0	239.0	143.6
3	202.3	121.6	262.4	157.7
4	197.8	118.9	257.7	154.9
5	202.5	121.7	253.7	152.5
6			245.7	147.7
7			240.1	144.3
8			242.6	145.8
9			242.1	145.5
Average	192.8	115.9	239.2	143.8

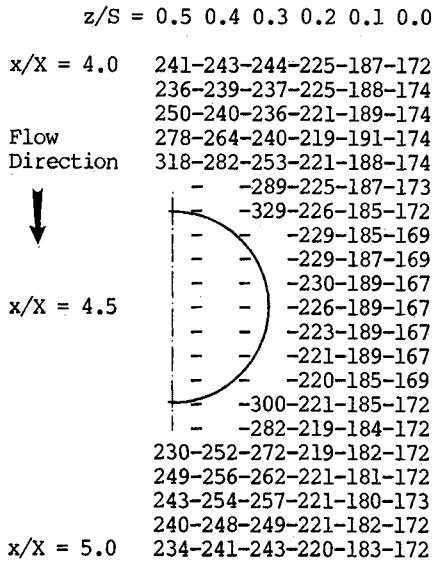

Fig. 9 Typical two-dimensional Sherwood number distribution, case 3.

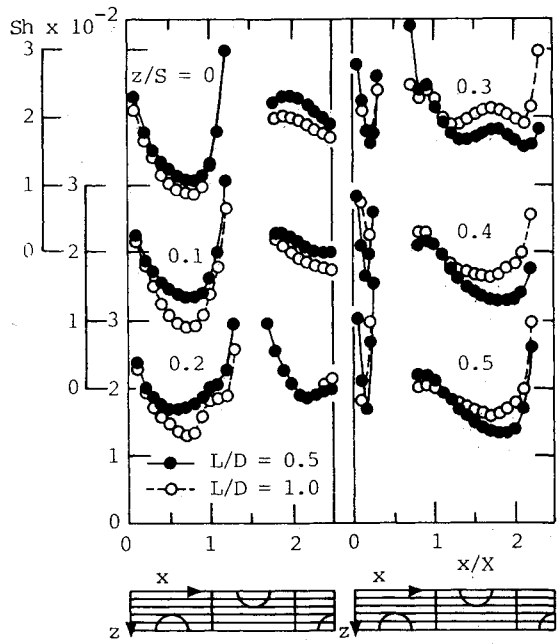

Fig. 10 Streamwise Sherwood number distributions, cases 1 and 4.

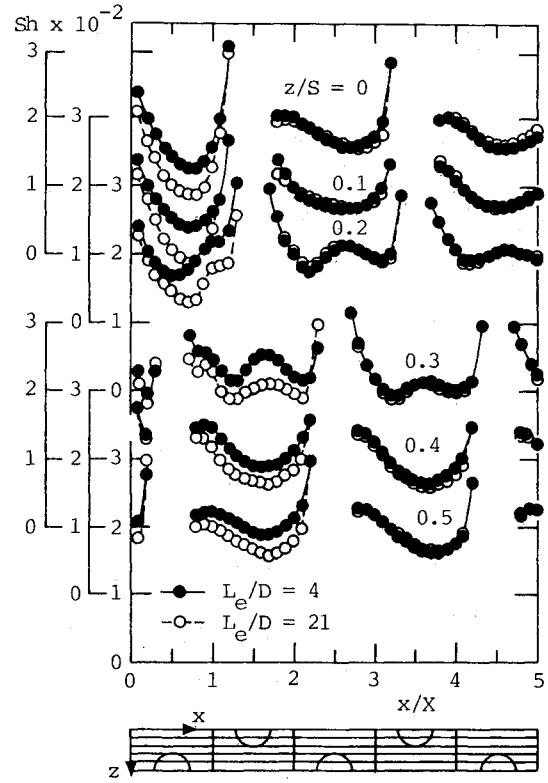

Fig. 11 Streamwise Sherwood number distributions, cases 1 and 5.

In comparing the corresponding distributions along $z/S = 0.3$, 0.4, and 0.5 in Figs. 6 and 8, the most noticeable difference is the absence of peaks in the distribution along $z/S = 0.3$ for $x/D \geq 1.5$ in the latter case.

The two-dimensional Sherwood number distribution for case 3 is shown in Fig. 9. The almost constant Sherwood number distributions along $z/S = 0$, 0.1, and 0.2 are evident. The Sherwood numbers along $z/S = 0$ are smaller than those along $z/S = 0.1$, which, in turn, are smaller than those along $z/S = 0.2$. The Sherwood numbers are again very large upstream of a pin, but are slightly smaller than those in the two previous cases in the wake downstream of a pin.

Pin Length-to-Diameter Ratio Effect

The effect of the pin length-to-diameter ratio on the local heat/mass transfer is illustrated in Fig. 10, in which the Sherwood number distributions for both $L/D = 1.0$ (case 1) and 0.5 (case 4) are plotted. Examination of Fig. 10 reveals that all segments of the distributions in the two cases are very similar. The distributions along $z/S = 0$, 0.1, and 0.2 in case 4 are always higher than those in case 1. The reverse is true for the distributions along $z/S = 0.3$, 0.4, and 0.5.

It must be pointed out that, in case 4, there are only three rows of pins (three alternate rows of three and two pins) in the array. It was necessary to limit the number of pins in the array so that the same S/D and X/D ratios of 2.5 were maintained for direct comparison of results and the same test channel could be used to conduct the experiments. As a result, the spanwise-averaged flow velocity varies significantly from row to row. For instance, the average velocity at $x/X = 1.5$ is about 82% of that at $x/X = 0.5$ due to the different amount of blockage to the flow at the two axial locations. The lower velocity at the second pin row may have caused the local Sherwood number distributions between $x/X = 1.0$ and 2.0 to have lower values than those in case 1.

Entrance Length Effect

Figure 11 demonstrates the effect of the length of the entrance duct on the heat/mass transfer in a pin fin channel.

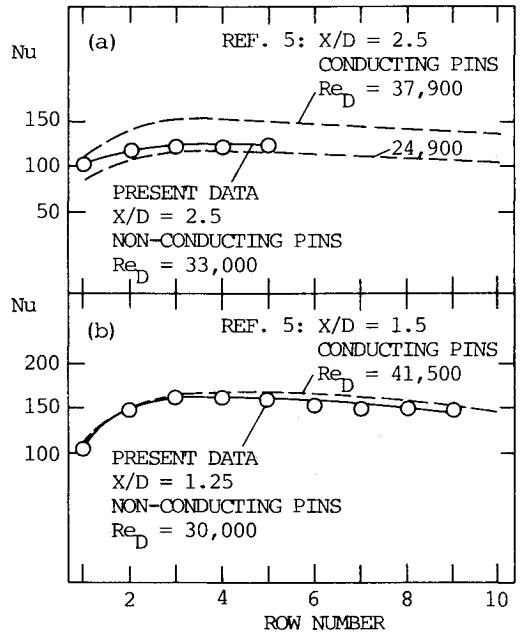

Fig. 12 Row-average Nusselt number distributions: a) case 1; b) case 2.

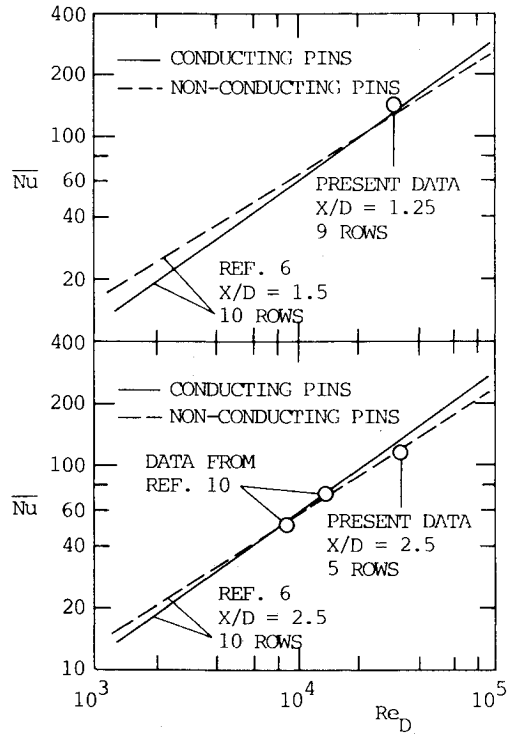

Fig. 13 Overall Nusselt numbers as functions of Reynolds number.

In Fig. 11, the black circular symbols and the open circular symbols are for $L_e/D = 4$ (the short entrance case) and 21 (the long entrance case), respectively. Near the leading edge, the Sherwood number distributions for $L_e/D = 4$ are consistently higher than those for $L_e/D = 21$, due to the thinner hydrodynamic boundary layer in the former case. Downstream of the third pin, the two Sherwood number distributions are essentially the same. Therefore, the effect of the entrance length on the heat/mass-transfer coefficient is limited to the first two rows of pins in a pin fin channel.

Average Sherwood Number

In order to compare the present local heat/mass-transfer results with the available average heat-transfer data, the spanwise-averaged Sherwood numbers by rows were determined using two sets of the local Sherwood number data—those of cases 1 and 2. The average Nusselt numbers were then calculated using Eq. (16) of Ref. 8. The exponent m in the equation was set equal to 0.4.

The results, which are given in Table 2, show that the spanwise-averaged Nusselt numbers in case 2 ($X/D = 1.25$) are generally higher than those in case 1 ($X/D = 2.5$). The axial development of the Nusselt numbers for the two cases are shown in Fig. 12, where the heat-transfer data from Ref. 5 are also included for comparison. From Fig. 12a, it is evident that the present data of case 1 for $X/D = 2.5$, $Re_D = 3.3 \times 10^4$, and nonconducting pins compare very well with those from Ref. 5 for the same X/D, $Re_D = 3.79$ and 2.49×10^4, and conducting pins. In Fig. 12b, the increasing then decreasing trend of the present data of case 2 is consistent with those of Ref. 5.

The overall Nusselt numbers for cases 1 and 2 are shown in Fig. 13, where the overall Nusselt numbers (over 10 pin rows) as functions of the flow Reynolds number from Ref. 6 for conducting and nonconducting pins and for $X/D = 1.5$ and 2.5 are also plotted. Again, the present data of cases 1 and 2 agree with the heat-transfer data very well. From Ref. 6, the overall Nusselt number for a channel with $X/D = 1.5$ and 10 rows of nonconducting pins is approximately 131 ($Re_D = 3.0 \times 10^4$, read from Fig. 4 of Ref. 6). The overall Nusselt number for case 2 (nine pin rows, $X/D = 1.25$) in the present study is 143.8. The 10% increase in heat transfer is believed to be the result of the smaller X/D ratio used in the present study. The average Nusselt number of 115.9 for case 1 (five pin rows, $X/D = 2.5$) in the present study is within 4% of the corresponding average Nusselt number of about 121 read from Fig. 5 of Ref. 6. Despite the fact that the Nusselt number was for five pin rows in case 1 and was averaged over 10 pin rows in Ref. 6, the two overall Nusselt number values are very nearly the same because of the relatively flat and increasing-then-decreasing profiles of the row-averaged Nusselt number distribution curves.

Concluding Remarks

The effects of the pin configuration, the pin length-to-diameter ratio, and the entrance length on the local endwall heat/mass transfer in a channel with short pin fins have been studied. Experimental results were obtained for staggered and aligned arrays of pin fins with $L/D = 0.5$ and 1.0, for $S/D = 2.5$, and for $X/D = 1.25$ and 2.5. The Reynolds numbers were kept at about 3.3×10^4. It was found that reducing the streamwise pin spacing in a staggered array increases the endwall heat/mass transfer. The local Sherwood number distributions for a staggered array and for an aligned array are very different from that for a plain channel with no pin fin and from each other. The effect of the entrance length on the endwall heat/mass transfer in a channel with a staggered array of pin fins is limited to the small region near the leading edge. The spanwise-averaged and overall data compare very well with previously published data.

Acknowledgment

This research was performed under the auspices of the National Science Foundation under Grant MEA 83-00722.

References

[1] Zukauskas, A., "Heat Transfer from Tubes in Crossflow," *Advances in Heat Transfer*, Vol. 8, 1972, pp. 93–160.

[2] Webb, R.L., "Air-Side Heat Transfer in Finned Tube Heat Exchangers," *Heat Transfer Engineering*, Vol. 1, 1980, pp. 33–49.

[3] VanFossen, G.J., "Heat-Transfer Coefficients for Staggered Arrays of Short Pin Fins," *Journal of Engineering for Power*, Vol. 104, 1982, pp. 268–274.

[4] Brigham, B.A. and VanFossen, G.J. Jr., "Length to Diameter Ratio and Row Number Effects in Short Pin Fin Heat Transfer,"

Journal of Engineering for Gas Turbines and Power, Vol. 106, 1984, pp. 241–245.

[5]Metzger, D.E., Berry, R.A., and Bronson, J.P., "Developing Heat Transfer in Rectangular Ducts with Staggered Arrays of Short Pin Fins," *Journal of Heat Transfer*, Vol. 104, 1982, pp. 700–706.

[6]Metzger, D.E. and Haley, S.W., "Heat Transfer Experiments and Flow Visualization for Arrays of Short Pin Fins," ASME Paper 82-GT-138, 1982.

[7]Simoneau, R.J. and VanFossen, G.J. Jr., "Effect of Location in an Array on Heat Transfer to a Short Cylinder in Crossflow," *Journal of Heat Transfer*, Vol. 106, 1984, pp. 42–48.

[8]Saboya, F.E.M. and Sparrow, E.M., "Local and Average Transfer Coefficients for One-Row Plate Fin and Tube Heat Exchanger Configurations," *Journal of Heat Transfer*, Vol. 96, 1974, pp. 265–272.

[9]Saboya, F.E.M. and Sparrow, E.M., "Transfer Characteristics of Two-Row Plate Fin and Tube Heat Exchanger Configurations," *International Journal of Heat and Mass Transfer*, Vol. 19, 1976, pp. 41–49.

[10]Lau, S.C., Kim, Y.S., and Han, J.C., "Local Endwall Heat/Mass Transfer in a Pin Fin Channel," *Heat Transfer and Fluid Flow in Rotating Machinery*, Hemisphere, Washington, 1987, pp. 64–75.

[11]Kline, S.J. and McClintock, F.A., "Describing Uncertainties in Single-Sample Experiments, *Mechanical Engineering*, Vol. 75, 1953, pp. 3–8.

[12]Sparrow, E.M. and Cur, N., "Turbulent Heat Transfer in a Symmetrically or Asymmetrically Heated Flat Rectangular Duct with Flow Separation at Inlet," *Journal of Heat Transfer*, Vol. 104, 1982, pp. 82–89.

[13]Goldstein, R.J. and Karni, J., "The Effect of a Wall Boundary Layer on Local Mass Transfer from a Cylinder in Crossflow," *Journal of Heat Transfer*, Vol. 106, 1984, pp. 260–267.